Scripta Materialia 255 (2025) 116368

Contents lists available at ScienceDirect

Scripta Materialia

journal homepage: www.journals.elsevier.com/scripta-materialia

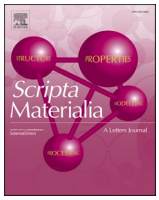

# Chemical strengthening of glass powder particles

Malcolm Schaenen [a], Qi Tang [a], Jianxiong Li [a], Mostafa Hassani [a,b,*]

[a] Sibley School of Mechanical and Aerospace Engineering, Cornell University, Ithaca, NY 14853, USA
[b] Department of Materials Science and Engineering, Cornell University, Ithaca, NY 14853, USA

ARTICLE INFO

*Keywords:*
Chemical strengthening
Glass
Powder
Particle compression
Fracture

ABSTRACT

It is well known that chemical strengthening of glass brings the benefit of increased fracture strength. Despite extensive research on processing and mechanics at the macroscale, the effectiveness of chemical strengthening on glass elements with all three dimensions in the micrometer regime remains largely unexplored. Here, we develop a novel process for chemical strengthening of micrometer-sized spherical glass powder particles and study the fracture behavior of these particles with in-situ particle compression tests inside a scanning electron microscope. Cross-sectional microscopy and energy dispersive spectroscopy measurements confirm ion exchange and show an increase in diffusion depth with an increase in processing time and temperature. We report a higher fracture strength for chemically strengthened powder particles compared with the as-received ones. We show that the increase in fracture strength is associated to the compressive residual stress resulting from ion exchange during chemical strengthening.

Although glass is a widely used engineering material, its brittle nature compromises its range of applications [1,2]. This is due to surface flaws found in glass that grow rapidly under tensile stress [3–6]. To counteract this, the chemical strengthening of glass can induce compressive stresses, thereby increasing the fracture strength and expanding its applications [7,8]. Chemically strengthened (CS) glass is widely used in sectors such as aerospace, motor, military, electronics and communications [9]. While the benefits of chemical strengthening on macroscale components, e.g., glass plates [10] and touch screens [11], are well-documented, its effects on microscale elements remains largely unexplored. The extent to which chemical strengthening may be applicable or even effective at the microscale has not been investigated. In this work we explicitly address this gap by chemical strengthening of microscale glass powder particles and in-situ studies of their fracture behavior.

Microscale glass powders (microspheres) are increasingly used as fillers and composites in the additive manufacturing of polymers [12,13], metals [14,15], and concrete [16]. Additionally, glass microspheres can be used in ball bearings [17] and as a raw material for additive manufacturing of glass [18]. The strength of these particles is critical as low fracture strengths can decrease the overall strength of the composite material and results in undesired deformation and failure [19,20]. Additionally, if the fracture strength of these microspheres is low, they can fracture during mixing [21]. The studies of fracture strength of glass particles in both cement [22] and synthetic foams [23,24], demonstrate that certain glass compositions with higher fracture strengths have led to higher overall tensile and compressive strengths. The strength of glass beads is also critical in the hydrofracturing applications as they serve as proppants. Research is currently focused on increasing the strength of these spheres as their premature fracture reduces proppant pack conductivity and decreases hydrocarbon production. Some strengthening methods currently include coating the beads with polymeric surface coatings to increase crushing strengths [25]. Certain studies into cold spray applications have also shown that harder reinforcement particles can be used to create composites with better surface wear resistance, [26] and better tensile strengths [27]. To this end it is important to develop methods to increase the fracture strength of glass microspheres thereby expanding their applications.

The focus of this study is to explore the possibility of chemically strengthening glass powder particles effectively. First, we developed a novel process for chemically strengthening powders. We used cross-sectional microscopy to characterize the chemically strengthened glass powder particles and confirm the occurrence of ion exchange. We have also conducted in-situ particle compression experiments inside a scanning electron microscope (SEM) to measure the strength of glass particles. Finally, the experimental measurements of strengthening results were compared to theoretical predictions of residual stress to explain the underlying mechanisms behind the achieved strengthening.

* Corresponding author.
*E-mail address:* hassani@cornell.edu (M. Hassani).

https://doi.org/10.1016/j.scriptamat.2024.116368
Received 3 May 2024; Received in revised form 29 August 2024; Accepted 4 September 2024
Available online 12 September 2024

Glass powders used in this experiment were solid soda lime glass microspheres in a range from 10 to 38 μm purchased from CoSpheric (Goleta, CA). To the best of our knowledge, there is no previous literature on the chemical strengthening of glass powders. This could be in part due to challenges in separating micrometer sized glass powder from molten potassium nitrate in traditional chemical strengthening processes [28]. In this study, glass particles were poured into the molten potassium nitrate solution. The target temperature was maintained for a specific holding time and then removed from the furnace to cool down to room temperature. Upon cooling, the potassium nitrate solidified with the glass powder. The solidified mixture was placed into a large glass of distilled water. The potassium nitrate readily dissolves in water while the glass is insoluble in water, leaving the powder to accumulate at the bottom of the glass. The solution was then poured through a funnel with grade 3 filter paper, allowing separation of the glass particles from the liquid solution (see the schematic Fig. S1 in supplementary material). We used a range of temperatures from 365 °C to 450 °C together with a range of times from 0.5 to 4 h in this work.

The CS particles were mixed into 6 g of carbon powder (MetLab CAT #M134), and hot pressed to make a solid carbon thermoset with glass particles embedded throughout the solid. The sample was then ground and polished to create a clean cross-section across the midplane of the particle. This cross-section was analyzed by Tescan Mira3 FESEM using an Energy Dispersive Spectroscopy (EDS) scan to find the concentration profile for the glass samples [29,30]. Particles with diameter of a 25–35 μm were chosen to study diffusion as they provided better resolution and accuracy on the concentration profiles. The concentration profiles were used to fit the diffusion coefficients of glass.

To experimentally measure the strengthening, particles were compressed using an Alemnis nano-indenter within a Zeiss LEO 1550 FESEM. A 10 μm diamond flat punch tip was used to compress the particles on a sapphire substrate. Due to the limitation of maximum load capability of the nano-indenter, particles between 10 and 15 μm were chosen from each sample for compression and were compressed at a rate of 8 mN/s. The load and displacement data were recorded until fracture was achieved. These measurements were repeated 10 times for both the as-received and the CS samples.

Exemplar EDS maps for CS particles are shown in Fig. 1(a-d). The sodium mapping presents a large concentration of sodium ions throughout the glass that is diminished at the surface of the glass particle. The potassium mapping shows that the potassium ions were successfully diffused into the glass particle at the surface, replacing the sodium ions. We fitted the concentration measurements from the EDS analysis using the concentration profile for diffusion in a sphere [31], Eq. (1), to find the diffusion coefficient:

$$\frac{C}{C_s} = 1 + \frac{2(d/2)}{\pi r}\sum_{n=1}^{\infty}\frac{(-1)^n}{n}\sin\left(\frac{n\pi r}{(d/2)}\right)\exp\left(-\frac{Dn^2\pi^2 t}{(d/2)^2}\right) \quad (1)$$

where $C$ is the concentration, $r$ is the radial position from the center of the glass sphere, $d$ is the particle diameter, $C_s$ is the concentration at the surface of the sphere, $D$ is the diffusion coefficient and $t$ is the time. Additionally, with the measurement conducted for chemical strengthening at different temperatures, we calculated the activation energy for alkali diffusion using Eq. (2):

$$D = D_o e^{-E_a/RT} \quad (2)$$

Where $D$ is the diffusion coefficient, $D_o$ is a constant, $R$ is the universal Gas constant, $T$ is the temperature (K), and $E_a$ is the activation energy for alkali diffusion.

The comparison of concentration of potassium as a function of distance from the surface between CS particles from different process parameters is shown in Fig. 1e. We observe that the potassium concentration across the particle increases as either the temperature or time of the chemical strengthening processing increases. With the same processing time, 1 h, lower temperature conditions such as 365 °C leads to smaller diffusion depths, creating a sharper concentration gradient. Higher temperature conditions such as 450 °C leads to a greater diffusion distance, creating a smoother concentration gradient. The same behavior is observed when increasing the time of the process while keeping the temperature constant. We can show that the diffusion data indeed obeys Eq. (1) by defining the dimensionless time, $\tau$, and dimensionless radial distance, $r^*$, as:

$$r^* = \frac{r}{(d/2)} \quad (3)$$

$$\tau = \frac{Dt}{(d/2)^2} \quad (4)$$

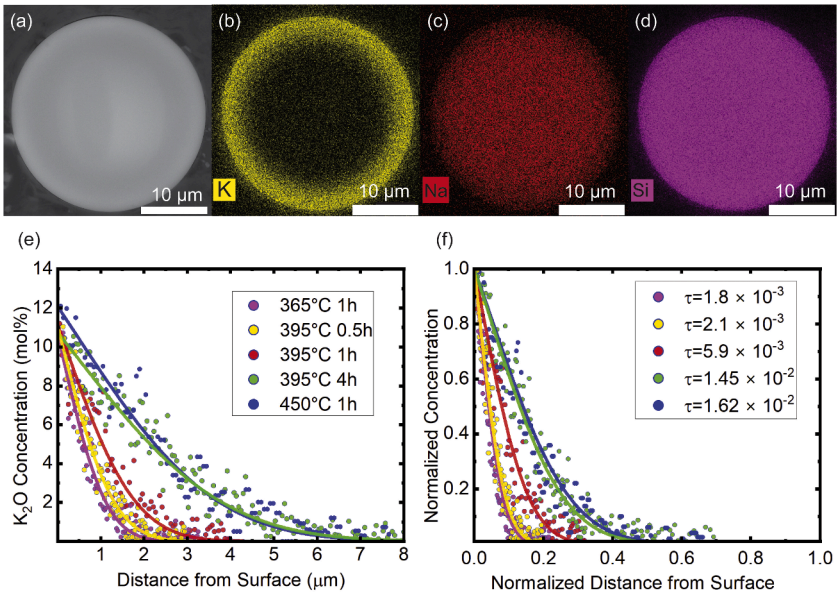


**Fig. 1.** Cross-sectional SEM images and elemental analysis of glass particle chemically strengthened at 395 °C for 4 h, (a) SEM image, (b) Potassium elemental map, (c) Sodium elemental map, (d) Silicon elemental map. (e) Measured Potassium vs. Distance from Surface, from EDS line scan of CS particles for different processing conditions, (f) Normalized Concentration values vs. Normalized Distance from Surface.

where $r$ is the radial distance from the center of the particle, $d$ is the particle diameter, $D$ is the diffusion coefficient, and $t$ is the process time. In Fig. 1f we observe a collapse of normalized concentration, $\frac{C}{C_s}$, for similar values of dimensionless time and normalized distance from the surface ($1\text{-}r^*$). Further analysis of the data results in an activation energy of $E_a = 100 \pm 5$ KJ/mol and $D_o = 1.8 \times 10^{-8}$ m$^2$/s from our experiments which closely align with the range of previously reported values from literature [32,33].

We used in-situ particle compression to measure the fracture strength of the glass particles. Fig. 2 shows snapshots of the particle compression during which a glass particle flattens slightly in between a rigid indenter and rigid substrate until fracture occurs. We can also observe the fractured surface of the particle parallel to the compression axis in Fig. 2. The fact that fracture occurs through particle splitting in half suggests a mode I fracture driven by tensile stresses perpendicular to the fracture surface. Following Hiramatsu and Oka's approach [34,35], we calculate the maximum tensile stress in a sphere under diametral compression by Eq. (5) which we can further consider to the fracture strength:

$$\sigma_f = \kappa \times \frac{4F_f}{\pi d^2} \tag{5}$$

Where $\sigma_f$ is the stress at fracture, $F_f$ is the force at fracture, and $\kappa$ is a constant that depends on the location of the maximum stress and material properties. This theoretical equation has been used to measure and compare the tensile strength in glass spheres, [36–38] and other brittle spheres [39–41], when diametrically compressed. The values for $\kappa$ used in diametral compression testing have been contested and different models and theories have been proposed based on material properties and loading conditions [42]. For glass, which is dominated by surface flaws, maximum tensile stress to cause fracture would be either located at the surface point just outside the contact area [43,44], or at the equatorial axis of the particle [45,46]. The location of the maximum tensile stress is dependent on the size of the radius of contact, $a_c$. Previous works have validated that when, $\frac{a_c}{(d/2)} \geq 0.65$, the maximum tensile stress in a sphere will be found at the surface near the equator [46–48]. From the image of the fractured particle, we observe that the radius of contact is 3.6 μm giving us an $\frac{a_c}{(d/2)} = 0.72$, therefore fracture will initiate along the equatorial axis. As such, we set the constant as 0.4 and assumed the maximum tensile stress as a hoop stress along the equatorial axis of the particle, causing a particle to be split in half along the axis of compression. Additionally, from the work of Shipway et al. [46] it has been stated that the tensile stress just outside the contact zone in unlikely to lead to catastrophic failure as there is a zone of compression present between the center of the sphere and the surface tensile region. This would cause a crack to grow in the circumferential direction producing a cone crack. Previous studies have shown that this tensile stress has led to spalling around the contact zone but indicated that it had no effect on the eventual catastrophic fracture [49,50]. These theories are further supported by our results found later in Fig. 3b as the values for stress on the sphere fit well with the expected theoretical values for surface stress.

During the immersion of glass powder particles in molten potassium nitrate, smaller sodium ions from the glass surface are exchanged with larger potassium ions from the molten salt. This ion exchange process creates a compressive residual stress layer on the glass surface, as the incoming potassium ion attempts to expand the glass matrix. This dimension change is quantified by the linear network dilation coefficient, $B$, which indicates the linear strain per unit change in concentration. Using an analogy between concentration and temperature gradient-induced dimensional change and residual stress generation, we can estimate the circumferential component of residual stress generated in a sphere from chemical strengthening with Eq. (6) [7,51,52]:

$$\sigma_{res}(r) = \left(\frac{BE}{1-\nu}(C(r,t) - \overline{C})\right) \tag{6}$$

Where $\sigma_{res}$ is the residual stress at radial positions from the center of the glass sphere (where positive values corresponds to compressive stress), $B$ is the linear network dilation coefficient of expansion, $E$ is the elastic modulus of the glass, $\nu$ is the poisons ratio of the glass, $C(r,t)$ is the concentration of potassium at a point $r$ from the center of the sphere, and $\overline{C}$ is the average concentration of potassium throughout the glass:

$$\overline{C} = \frac{3}{(d/2)^3}\int_0^{d/2} Cr^2 dr \tag{7}$$

The value for $E$ used in Eq. (6), was determined as 74 GPa through the fitting of the linear elastic segment of the particle compression load-displacement data, following the linear elastic Hertzian contact theory [53,54]. This falls in line with what is expected for SLS glass [55]. The values for the linear network dilation coefficient were taken from the work of Sun and Dugnani [56]. For reference at a molar percent of $K_2O$=11 mol% the linear network dilation coefficient was $B = 4.70 \times 10^{-4}$ mol%$^{-1}$ and when $K_2O$=12 mol% the linear network dilation coefficient was $B = 4.47 \times 10^{-4}$ mol%$^{-1}$. Poisson's ratio was taken as $\nu = 0.22$ [57]. Finally, $C_s$ was given as a value of 11.5 mol%, an average value of experimental measurements.

As glass has a distribution of surface flaw sizes, the strength must be estimated using a three parameter Weibull Distribution, which is suggested as being more suitable for the compression of glass spheres, [1,37,48,58]:

$$P = 1 - \exp\left[-\left(\frac{\sigma_f - \sigma_\mu}{\sigma_o}\right)^m\right] \tag{8}$$

Where $P$ is the probability of fracture, $\sigma_o$ is the characteristic fracture strength where $P = 63$ %, $\sigma_\mu$ is the location parameter, and $m$ is the shape factor.

Using Eqs. (5) and (8) we measured the characteristic fracture strength from the as-received particles and compared them to the characteristic fracture strength of each CS sample. Weibull plots were created for each processing condition for a sample size of 10 particles shown in Fig. 3a. For the as-received samples we obtained a characteristic fracture strength of 969 MPa. Within the range of times and temperatures tested, our measurements show that chemical strengthening process indeed increased the fracture strength of the glass with the increases in characteristic fracture strength reaching as high as 1308 MPa. For each different CS sample tested, as the time or temperature decreased, the characteristic fracture strength increased. The CS

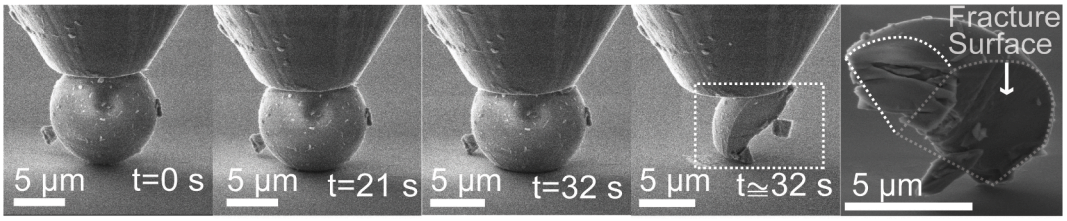


**Fig. 2.** Snapshots of the in-situ glass particle compression test inside SEM, along with a close-up view of the fractured particle.

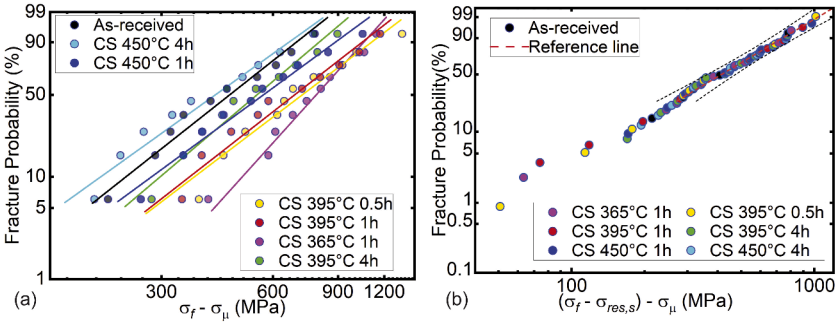


**Fig. 3.** (a) Weibull Distribution of the fracture strengths of the as-received and chemically strengthened glass particles. (b) Weibull Distribution of the fracture stress subtracted by the residual stress of the glass particles.

particles processed at 365 °C for 1 h showed the highest fracture strengths shown in Fig. 3a.

While it has been reported that the electron beam may influence the mechanical properties of glass [59,60], the effect is limited to very small particles in the nanoscale range of 200 nm [60] under a high energy, 300 kV, TEM. The effect of the electron beam has been also shown to be limited in the microscale range 1–5 μm [59] under lower energy, 5–10 kV SEM. As the penetration depth of the CS sample was in the 1–2 μm range, and we had a low beam intensity of 5 kV, we expect a negligible effect from the electron beam on the measured fracture strengths.

Under the assumptions that the crack size does not change after the chemical strengthening process, and that the unstable crack propagates from an existing surface flaw (see supplementary information, section 2) [61], we expect the increase in fracture strength to align with the compressive residual stress present at the surface:

$$\sigma_{f,CS} - \sigma_{f,AR} = \sigma_{res,s} \tag{9}$$

Where $\sigma_{f,CS}$ is the fracture strength of CS particles, $\sigma_{f,AR}$, is the fracture strength of the as-received particles and $\sigma_{res,s}$ is compressive residual stress at the surface for the corresponding chemical strengthening conditions. To confirm the role of residual stress in increasing the fracture strength (Eq. 9), we subtracted the theoretical residual stress from the fracture strength of each set of CS glass particles. Fig. 3b shows that when the residual stress is subtracted, all the data collapses into a single Weibull plot expected for the as-received glass. The characteristic fracture strength from Fig. 3b, 945 MPa, is also in good agreement with the characteristic fracture strength taken from the Weibull plot of the as-received glass in Fig. 3a which was 969 MPa. The reference line shows the theoretical best fit Weibull distribution line for the collated data. A 95 % confidence band was shown around the plot. The shape is in accordance with what we would expect on a Weibull graph from previous studies on the compression of glass spheres [62]. From this data set the location parameter was found to be 449 MPa. The location parameter is estimated from the data, by maximizing the coefficient of determination from the linear regression [58].

Fig. 4 shows a map of surface residual stress for a particle size of 12 μm as a function of chemical strengthening time and temperature calculated using Eqs. (6) and Eq. (1). The parameters for Eq. (1) were taken from the diffusion properties found from the EDS analysis. Although the EDS characterizations were conducted on 25–35 μm particles, since diffusion properties are intrinsic material properties, they can be used to predict the diffusion behavior of smaller particles as well. The surface residual stress decreases as the processing time and temperature increases. With higher temperature and longer processing time, ion exchange propagates towards the center of the particle, leading to an increase in the average concentration level, and as a result a decrease in surface residual stress. We have superimposed the strengthening, i.e., the left-hand side of Eq. (9) (which we measured experimentally for all the studied processing conditions) with circles on the surface residual stress map of Fig. 4 predicted theoretically. The average particle size and

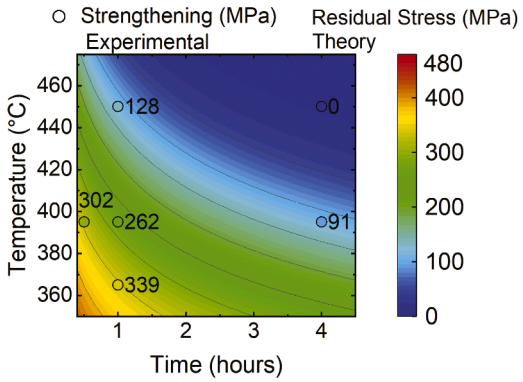


**Fig. 4.** Theoretical residual stress map as a function of time and temperature. Experimental measurements of strengthening for the chemically strengthened particles are also superimposed on the map.

the standard deviation for all the particles tested in this work are 12 ± 1 μm. Once again, the close agreement between the theoretical predictions of residual stress and the experimental measurement of strengthening confirms that the increase in fracture strength can indeed be attributed to surface compressive residual stress generated due to the ion exchange during the process.

While only particles with diameter of 10–15 μm were tested in this study due to the limitation of our loading cell, we can use the theoretical framework presented above to discuss the effects of particle size on the strengthening of glass particles. We define a dimensionless diffusion length (described in the Supplementary Information) that combines both diffusion depth and particle size into a single parameter. This parameter helps analyze how particle size affects residual stress and the strengthening behavior. For a specific process parameter, Eq. (1) shows that the diffusion depth of potassium ions remains relatively constant across different particle sizes as long as the particles are not small enough for ion saturation. Therefore, as particle size increases and the dimensionless diffusion length decreases, the potassium ion concentration profile represents a smaller fraction of the ions within the glass particle, leading to a reduction in the average potassium ion concentration (Eq. (7)). Finally, the lower level of average potassium ion concentration results in a higher residual stress at the surface of the glass particle (Eq. (6) and Fig. S2). The increase in residual stress with larger particle sizes is more pronounced for process parameters that result in greater diffusion depths (e.g., 395 °C for 4 h and 450 °C for 1 h). This is because a greater diffusion depth can cause a higher ion concentration in smaller glass particles, which reduces the surface residual stress.

In line with the results shown in Figs. 1 and 3a, we also observe in the map of Fig. 4 that the strengthening effects diminish at higher temperatures and longer duration of the chemical strengthening process within the times and temperatures tested. As time and temperature increase,

there is a greater exchange of ions throughout the particle. This increases the average concentration of the particle. The closer the surface concentration is to the average concentration, the weaker the strengthening will be as predicted in Eq. (6). The difference in concentration between the surface and the average concentration leads to the difference in strain between the layers, creating the residual stress. When the ions diffuse deeply into the particle, the entire particle will begin to expand to accommodate the ions. This leads to a smaller difference in strain between the surface and the rest of the particle, and thus a smaller stress value [52]. In microparticles where the overall size is on the same scale as the depth of ion penetration, the ion exchange process can increase the overall concentration, reducing the strengthening. It should be noted that as time and temperature continue to decrease, we will expect to reach a lower threshold where there will be a significant decrease in the maximum surface concentration [32], leading to a decrease in strength.

In summary, we developed a novel process for the chemical strengthening of micrometer-sized glass powder particles. We confirmed potassium ion exchange in glass powder particles through cross-sectional scanning electron microscopy observations and energy dispersive spectroscopy analysis. The diffusion depth was shown to increase with processing time and temperature. We measured the fracture strength of glass powder particles with in-situ particle compression tests inside a scanning electron microscope. Our measurements confirmed considerable strengthening achieved in chemically strengthened particles. We demonstrated that experimental measurements of strengthening closely align with the magnitude of the surface compressive residual stress resulting from the potassium ion exchange during the process. We systematically explored the chemical strengthening process parameter space and revealed that the essence of improving glass particle fracture strength lies in the precise control of the ion exchange process to prevent excessive ion exchange. This work could provide insights into improving the fracture strength of glass powder particles, thereby broadening their applications.

## CRediT authorship contribution statement

**Malcolm Schaenen:** Writing – review & editing, Writing – original draft, Visualization, Methodology, Investigation, Formal analysis, Data curation. **Qi Tang:** Writing – review & editing, Methodology, Investigation, Formal analysis, Data curation. **Jianxiong Li:** Writing – review & editing, Methodology, Investigation, Formal analysis, Data curation. **Mostafa Hassani:** Writing – review & editing, Supervision, Methodology, Funding acquisition, Formal analysis, Conceptualization.

## Declaration of competing interest

The authors declare that they have no known competing financial interests or personal relationships that could have appeared to influence the work reported in this paper.

## Acknowledgments

Authors gratefully acknowledge funding received from National Science Foundation (CMMI-2330319). Authors also acknowledge the use of facilities and instrumentation supported by NSF through the Cornell University Materials Research Science and Engineering Center DMR-1719875.

## Supplementary materials

Supplementary material associated with this article can be found, in the online version, at doi:10.1016/j.scriptamat.2024.116368.

## References

[1] A.K. Varshneya, J.C. Mauro, Strength and toughness, in: A.K. Varshneya, J. C. Mauro (Eds.), Fundamentals of Inorganic Glasses, 3rd, Elsevier, 2019, pp. 487–535.
[2] B. Sugarman, Strength of glass (a review), J. Mater. Sci. 2 (1967) 275–283.
[3] S.W. Freiman, Fracture Mechanics of Glass, in: D.R. Uhlmann, N.J. Kreidl (Eds.), Glass Science and Technology, Elsevier, 1980, pp. 21–78.
[4] A.~A. Griffith, The phenomena of rupture and flow in solids, Philosophical Transactions of the Royal Society of London Series A 221 (1921) 163–198.
[5] F. Erdogan, Fracture mechanics, Int. J. Solids Struct. 37 (2000) 171–183.
[6] G.R. Irwin, Analysis of stresses and strains near the end of a crack traversing a plate, J. Appl. Mech. 24 (1957) 361–364.
[7] R. Gy, Ion exchange for glass strengthening, Mater. Sci. Eng.: B 149 (2008) 159–165.
[8] A.K. Varshneya, Chemical strengthening of glass: lessons learned and yet to be learned, Int. J. Appl. Glass Sci. 1 (2010) 131–142.
[9] S. Karlsson, B. Jonson, C. Stålhandske, The technology of chemical glass strengthening – A review, Glass Technology: Eur. J. Glass Sci. Technol. Part A 51 (2010) 41–54.
[10] Z. Wang, T. Suo, A. Manes, Effect of chemical strengthening residual stress on the flexural performance and fracture behavior of aluminosilicate glass, Eng. Fract. Mech. 258 (2021) 108104.
[11] J.-H. Maeng, D.-H. Kim, S.-M. Park, H.-J. Kim, The effect of chemical treatment on the strength and transmittance of soda-lime cover glass for mobile, Int. J. Precis. Eng. Manuf. 15 (2014) 1779–1783.
[12] L.C. Kontaxis, F.K. Kozaniti, G.C. Papanicolaou, Mechanical behavior modelling and filler geometry effect of glass filler reinforced starch-epoxy hybrid matrix composites, Materials (Basel) 14 (2021) 6587.
[13] N. Vidakis, M. Petousis, N. Mountakis, V. Papadakis, C. Charou, V. Rousos, P. Bastas, Glass fillers in three different forms used as reinforcement agents of polylactic acid in material extrusion additive manufacturing, Appl. Sci. 13 (2023) 6471.
[14] L. He, M. Hassani, A review of the mechanical and tribological behavior of cold spray metal matrix composites, J. Therm. Spray Technol. 29 (2020) 1565–1608.
[15] Z. Khalkhali, K.S. Rajan, J.P. Rothstein, Peening effect of glass beads in the cold spray deposition of polymeric powders, J. Therm. Spray Technol. 29 (2020) 657–669.
[16] G.M.S. Islam, M.H. Rahman, N. Kazi, Waste glass powder as partial replacement of cement for sustainable concrete practice, Int. J. Sustainable Built Environ. 6 (2017) 37–44.
[17] M.J. Samsel, A. Chańko, M. Michałowski, M. Fernandez-Munoz, E. Diez-Jimenez, Tribological characterization of micro ball bearings with and without solid-state lubrication, Micromachines (Basel) 14 (2023) 1775.
[18] C. Xin, Z. Li, L. Hao, Y. Li, A comprehensive review on additive manufacturing of glass: recent progress and future outlook, Mater. Des. 227 (2023) 111736.
[19] G. Loubrieu, M.Le Gall, D. Priour, G. Stewart, D. Melot, P.Y. Le Gac, Hydrostatic strength of hollow glass microspheres composites: influencing factors and modelling, Composites Part C: Open Access 8 (2022) 100286.
[20] J. Yang, L. Chen, Z. He, C. Li, B. Yu, Z. Wei, Z. Zhao, Z. Hao, High-strength hollow glass microsphere/epoxy resin composite insulation materials for deep in-situ condition preserved coring, Geofluids 2022 (2022) 1–10.
[21] S. Shira, C. Buller, Mixing and dispersion of hollow glass microsphere products, in: S.E. Amos, B. Yalcin (Eds.), Hollow Glass Microspheres For Plastics, Elastomers, and Adhesives Compounds, William Andrew Publishing, Oxford, 2015, pp. 241–271.
[22] N.R. Scott, D.L. Stoddard, M.D. Nelms, Z. Wallace, I. Turner, L. Turner, M. Croom, K. Franklin, S. Sandifer, M.S. Ali Al-fahdi, T. Butler, A.M. Rajendran, Experimental and computational characterization of glass microsphere-cementitious composites, Cem. Concr. Res. 152 (2022) 106671.
[23] N. Gupta, R. Nagorny, Tensile properties of glass microballoon-epoxy resin syntactic foams, J. Appl. Polym. Sci. 102 (2006) 1254–1261.
[24] N. Gupta, E. Woldesenbet, P. Mensah, Compression properties of syntactic foams: effect of cenosphere radius ratio and specimen aspect ratio, Compos Part A Appl Sci Manuf 35 (2004) 103–111.
[25] U. Ishtiaq, A. Aref, A.S. Muhsan, A. Rashid, S.S. Hamdi, High strength glass beads coated with CNT/rGO incorporated urethane coating for improved crush resistance for effective hydraulic fracturing, J. Pet. Explor. Prod. Technol 12 (2022) 2691–2697.
[26] C.J. Akisin, F. Venturi, M. Bai, C.J. Bennett, T. Hussain, Microstructure, mechanical and wear resistance properties of low-pressure cold-sprayed Al-7 Mg/Al2O3 and Al-10 Mg/Al2O3 composite coatings, Emergent Mater 4 (2021) 1569–1581.
[27] F.N. Lomo, A. Vargas-Uscategui, P.C. King, M.J. Patel, I.S. Cole, Microstructure and mechanical properties of heat-treated cold spray additively manufactured titanium metal matrix composites, J. Manuf. Process 99 (2023) 12–26.
[28] R. Forker, T. Kozlowski, D. Krygier, J. Panzarino, Chemically strengthened glass, US3773489A, 1971.
[29] E. Mognato, M. Schiavonato, A. Barbieri, M. Pittoni, Process influences on mechanical strength of chemical strengthened glass, Glass Structures & Engineering 1 (2016) 247–260.
[30] C. Fourmentin, X.-H. Zhang, E. Lavanant, T. Pain, M. Rozé, Y. Guimond, F. Gouttefangeas, L. Calvez, IR GRIN lenses prepared by ionic exchange in chalcohalide glasses, Sci. Rep. 11 (2021) 11081.
[31] J. Crank, The Mathematics of Diffusion, 2nd ed., Oxford University Press, London, 1975.

[32] F. Bengtsson, I.B. Pehlivan, L. Österlund, S. Karlsson, Alkali ion diffusion and structure of chemically strengthened TiO2 doped soda-lime silicate glass, J Non Cryst Solids 586 (2022) 121564.
[33] S. Karlsson, L. Wondraczek, S. Ali, B. Jonson, Trends in effective diffusion coefficients for ion-exchange strengthening of soda-lime-silicate glasses, Front Mater. 4 (2017).
[34] Y. Hiramatsu, Y. Oka, Determination of the tensile strength of rock by a compression test of an irregular test piece, Int. J. Rock Mech. Mining Sci. Geomechanics Abstracts 3 (1966) 89–90.
[35] Y. Oka, H. Majima, A theory of size reduction involving fracture mechanics, Can. Metall. Q. 9 (1970) 429–439.
[36] B.A. Kschinka, S. Perrella, H. Nguyen, R.C. Bradt, Strengths of glass spheres in compression, J. Am. Ceram. Soc. 69 (1986) 467–472.
[37] J. Huang, S. Xu, H. Yi, S. Hu, Size effect on the compression breakage strengths of glass particles, Powder Technol. 268 (2014) 86–94.
[38] I.G. Watkins, M. Prado, Mechanical properties of glass microspheres, Procedia Mater. Sci. 8 (2015) 1057–1065.
[39] M.K. Gundepudi, B.V. Sankar, J.J. Mecholsky, D.C. Clupper, Stress analysis of brittle spheres under multiaxial loading, Powder Technol. 94 (1997) 153–161.
[40] T. Hioki, A. Itoh, S. Noda, H. Doi, J. Kawamoto, O. Kamigaito, Effect of ion implantation on fracture stress of Al2O3, Nucl. Instrum. Methods Phys. Res. B 7–8 (1985) 521–525.
[41] K.T. Chau, X.X. Wei, R.H.C. Wong, T.X. Yu, Fragmentation of brittle spheres under static and dynamic compressions: experiments and analyses, Mech. Mater. 32 (2000) 543–554.
[42] G. Žagar, V. Pejchal, M. Kissling, A. Mortensen, On the diametric compression strength test of brittle spherical particles, Eur. J. Mech. A. Solids 72 (2018) 148–154.
[43] Y. Chen, A. Best, T. Haschke, W. Wiechert, H.-J. Butt, Stress and failure at mechanical contacts of microspheres under uniaxial compression, J. Appl. Phys. 101 (2007).
[44] K. Schönert, Breakage of spheres and circular discs, Powder Technol. 143–144 (2004) 2–18.
[45] P.H. Shipway, I.M. Hutchings, Fracture of brittle spheres under compression and impact loading. II. Results for lead-glass and sapphire spheres, Philos. Mag. A 67 (1993) 1405–1421.
[46] P.H. Shipway, I.M. Hutchings, Fracture of brittle spheres under compression and impact loading. I. Elastic stress distributions, Philos. Mag. A 67 (1993) 1389–1404.
[47] V. Pejchal, G. Žagar, R. Charvet, C. Dénéréaz, A. Mortensen, Compression testing spherical particles for strength: theory of the meridian crack test and implementation for microscopic fused quartz, J. Mech. Phys. Solids 99 (2017) 70–92.
[48] W.L. Lim, G.R. McDowell, A.C. Collop, The application of Weibull statistics to the strength of railway ballast, Granul Matter 6 (2004) 229–237.
[49] R.J. Verrall, A sphere compression test for measuring the mechanical properties of dental composite materials, J. Dent. 4 (1976) 11–14.
[50] N. Arbiter, Single fracture of brittle spheres, Soc. Min. Eng. AIME, Trans. 244 (1969) 118–133. https://cir.nii.ac.jp/crid/1573387450701028224.bib?lang=en. accessed July 23, 2024.
[51] A.R. Cooper, D.A. Krohn, Strengthening of glass fibers: II, ion exchange, J. Am. Ceram. Soc. 52 (1969) 665–669.
[52] S.P. Timoshenko, J.N. Goodier, H.N. Abramson, Theory of Elasticity, 3rd ed., McGraw-Hill, New York, 1970. Third.
[53] M.J. Puttock, E.G. Thwaite, Elastic Compression of Spheres and Cylinders at Point and Line Contact, Commonwealth Scientific and Industrial Research Organization, Melbourne, 1969.
[54] N.V. Silva, S.C. Angulo, A. da Silva Ramos Barboza, D.A. Lange, L.M. Tavares, Improved method to measure the strength and elastic modulus of single aggregate particles, Mater. Struct. 52 (2019) 77.
[55] T.P. Seward, T. Vascott, High Temperature Glass Melt Property Database For Process Modeling, The American Ceramic Society, Westerville, Ohio, 2005.
[56] H. Sun, R. Dugnani, A study on ion-exchanged, soda-lime glass's residual stress relationship with K+/Na+ concentration, Int. J. Appl. Glass Sci. 11 (2020) 134–146.
[57] E. Symoens, R. Van Coile, J. Belis, Experimental investigation into the effect of elevated temperatures on the fracture strength of soda-lime-silica glass, Glass Structures & Engineering 7 (2022) 457–469.
[58] Z. Han, L.C. Tang, J. Xu, Y. Li, A three-parameter Weibull statistical analysis of the strength variation of bulk metallic glasses, Scr. Mater. 61 (2009) 923–926.
[59] G. Kermouche, G. Guillonneau, J. Michler, J. Teisseire, E. Barthel, Perfectly plastic flow in silica glass, Acta Mater. 114 (2016) 146–153.
[60] M. Mačković, F. Niekiel, L. Wondraczek, E. Spiecker, Direct observation of electron-beam-induced densification and hardening of silica nanoballs by in situ transmission electron microscopy and finite element method simulations, Acta Mater. 79 (2014) 363–373.
[61] B. Egboiyi, R. Mattey, S. Konica, P. Nikam, S. Ghosh, T. Sain, Mechanistic understanding of the fracture toughening in chemically strengthened glass—Experiments and phase-field fracture modeling, Int. J. Solids Struct. 238 (2022) 111374.
[62] B. Dillinger, D. Clark, C. Suchicital, G. Wicks, Crush Strength Analysis of Hollow Glass Microspheres, in: Proceedings of the 41st International Conference on Advanced Ceramics and Composites, 2018, pp. 11–25.